Int. J. Electrochem. Sci., 17 **(2022)** Article Number: 220420, doi: 10.20964/2022.04.09

International Journal of
ELECTROCHEMICAL
SCIENCE
www.electrochemsci.org

Short Communication

Electrochemical Methods for Investigating the Relationship between Estrogen Receptors and PI3K Pathways in Breast Cancer Cells

Li Han[1,2] *and Bin Qiao*[3,*]

[1] Zhang Zhongjing College of Chinese Medicine, Nanyang Institute of Technology, Nanyang, 473004, China
[2] Henan Key Laboratory of Zhang Zhongjing Formulae and Herbs for Immunoregulation, Nanyang Institute of Technology, Nanyang, 473004, China
[3] College of Plant Protection, Northwest A&F University, Xianyang, Shanxi, 712100, China,
[*]E-mail: luckyhanlnyist666@163.com

Received: 8 December 2021 / *Accepted:* 17 January 2022 / *Published:* 4 March 2022

The estrogen receptor (ER) and phosphatidylinositol 3-kinase (PI3K) signaling pathways are critical in the progression and treatment of breast cancer. The level of ER expression and its association with the PI3K pathway are critical for predicting the efficacy of endocrine therapy in breast cancer and for understanding potential drug resistance mechanisms. Using molecular imprinting, capacitive, and electrochemical polymerization techniques, we developed an advanced sensor for ER detection. By hydrogen bonding the template molecule ER to the binding site, an imprinted membrane is formed on the electrode surface. This electrochemical biosensor is capable of detecting the level of ER expression in cells. The signal increases in proportion to the amount of ER present in the reaction solution. Under optimal conditions, the sensor detects ER concentrations ranging from 0.5 nM to 0.1 nM linearly, with a detection limit of 0.24 nM. After 6 hours of treatment with the PI3K inhibitor BEZ-235, the signal intensity was significantly increased compared to the DMSO-treated control, and the signal intensity was positively correlated with the inhibitor concentration.

Keywords: Estrogen receptor, PI3K pathway, EIS sensor, Molecular imprinting, Breast cancer

1. INTRODUCTION

Estrogen directly binds to two classes of estrogen receptors in the nucleus, ERα and ERβ, to regulate target gene transcription, which is the classical estrogen receptor signaling pathway [1,2]. Recently, it was discovered that estrogen receptors can also be activated through estrogen-dependent or estrogen-independent phosphorylation. The ligand-dependent and ligand-independent pathways,

respectively, are used to refer to these estrogen-dependent and estrogen-independent pathways [3–5]. Estrogen binding to ER can activate or repress enhancers in target gene regulatory regions and regulate target gene transcription by regulating the target gene's estrogen response element (ERE) in concert with coactivators [6,7]. Estrogen also acts on estrogen receptors on cell membranes and binds to a variety of cellular signaling molecules, including mitogen-activated protein kinase, phosphatidylinositol-3-kinase/protein serine threonine kinase (PI3K/Akt), and others, to exert rapid non-genomic effects via transmembrane signaling mechanisms [8–10].

The ERα, a member of the steroid hormone receptor superfamily, is composed of several structure-function domains, each of which contains a transcriptional activation function domain (AF), designated AF1 and AF2. The distinction is that AF1 functions as a non-ligand-dependent transcriptional activator, whereas AF2 functions as a ligand-dependent transcriptional activator. ERα-AF1 region contains four Ser-Pro motifs (Ser-104, Ser-106, Ser-118, Ser-167). Serine (Ser-236) and tyrosine (Tyr-537) residues in the DBD can also be phosphorylated by ligands or molecules involved in specific signaling pathways [5,11–14]. PI3K is composed of two subunits: a catalytic subunit with a molecular mass of 110×10^3 and a regulatory subunit with a molecular mass of 85×10^3. PI3K can be activated in two distinct ways. One is activated through interaction with growth factor receptors or linker proteins containing phosphorylated tyrosine residues, resulting in a change in the dimeric conformation [15–17]. The other is via direct interaction between the oncogene RaS and p110, which results in activation of P13K. When PI3K is activated, a second messenger, phosphatidylinositol 3 (PIP3), is produced at the plasma membrane. PIP3 interacts with the intracellular signaling protein Akt, facilitating its translocation from the cytoplasm to the cell membrane and acquisition of catalytic activity [18–23]. Phosphatidylinositol-dependent protein kinase (PDK) is involved, with PDK1 phosphorylating the Akt protein at position Thr308 and PDK2 phosphorylating the Akt protein at position Ser473. Akt's functional activity can be fully developed only when both Thr308 and Ser473 are phosphorylated. By phosphorylating Akt, it activates or inhibits its downstream proteins, thereby regulating cell proliferation, differentiation, apoptosis, and migration. At least three members of the Akt family have been identified thus far: Akt1/PKBα, Akt2/PKBβ, and Akt3/PKBγ [24,25]. They are regulated by three distinct genes, but share a common protein structure.

Breast cancer is the leading cause of death from cancer in women, accounting for 16% of new cancer cases in women. The ER performs its transcriptional function in response to the activation of signaling pathways by steroidal estrogens by binding directly to its own ERE or indirectly to other transcription factors, thereby initiating a series of cell growth events. There is mounting evidence that ER plays a significant role in breast cancer development [6,11,26]. ER is a critical therapeutic marker and target for breast cancer in clinical practice, as it is used to monitor associated pathological phenomena and treatment efficacy. Endocrine therapy targeting ER, as represented by tamoxifen, has become one of the most effective treatments for hormone receptor-positive breast cancer over the last two decades. However, endocrine therapy invariably results in drug resistance, reducing therapeutic efficacy significantly [27–29]. The PI3K pathway is a critical component of the growth factor signaling pathway and has been linked to endocrine resistance in breast cancer. Experimental and clinical evidence indicates that inhibiting the PI3K pathway can reverse endocrine resistance and that inhibiting both the PI3K and ER pathways can improve treatment outcomes. The PI3K pathway has been hypothesized to

interact with the ER pathway, resulting in ER downregulation or deletion, resulting in endocrine resistance [30]. However, some studies have demonstrated that the levels of mRNA expression do not always correspond to the levels of protein expression [31]. As a result, it is critical to continue investigating the quantitative effect of PI3K inhibitors on ER protein expression levels. We present an electrochemical sensor based on molecular imprinting technology in this work. Between the electrical impedance signal and ER proteins, a quantitative relationship can be established. This method has the advantages of simplicity, rapidity, sensitivity, and economy. We examined the level of ER expression in breast cancer cells treated with PI3K inhibitors in order to determine the relationship between the PI3K pathway and ER.

2. EXPERIMENTAL

2.1 Chemicals and instruments

p-mercaptoaniline (p-ATP), tetrabutylammonium perchlorate and chloroauric acid were purchased from Sigma. Potassium ferricyanide, potassium ferricyanide and potassium chloride were purchased from Xi'an Chemical Reagent Co. Ltd. Human recombinant estrogen receptor was purchased from Invitrogen, USA. The PI3K inhibitor NVP-BEZ235 (BEZ235) was supplied by LC, USA. Bovine serum albumin (BSA) was purchased from Dingguo Biotechnology Co. Ltd, China. Three breast cancer cells (MCF-7, MDA-MB-231 and BT-474) were purchased from the Institute of Cell Research, Shanghai Academy of Sciences. Nuclear Extraction Kit was purchased from Active Motif, USA. Unless otherwise specified, all reagents used were analytically pure.

The surface morphology of the prepared electrodes was observed using a Hitachi s-4800 scanning electron microscope (SEM, Electron Optics, Japan). Electrochemical impedance (EIS) experiments were performed on a multichannel electrochemical workstation (Princeton Instruments, USA). A three-electrode system was used for electrochemical measurements: a Ag/AgCl, a Pt wire and a gold electrode were used as the reference electrode, counter electrode and working electrode, respectively. The impedance spectra were recorded in the frequency range 1 Hz to 10,000 Hz at an ethanol acidic solution (pH 5.2). ZSimpWin software was used for data processing. All experiments were performed at room temperature.

2.2 Cell culture and preparation of nuclear extracts

Cells were cultured in DMEM medium supplemented with 10% fetal bovine serum and antibiotics at a concentration of 50 U/mL penicillin and 50 mg/mL streptomycin. Cells were cultured at 37°C in a humidified incubator containing 5% CO_2. Prior to the addition of drug intervention, cells were incubated in phenol red-free medium for 48 hours and then starved in serum-free medium overnight. A predetermined concentration of the PI3K inhibitor BEZ-235 (solubilized with DMSO) was added to the medium in triplicate for a predetermined period of incubation, followed by immediate nucleolysis. As a

control, DMSO was used. Before preparing nuclear extracts, cells from both the experimental and control groups were washed twice with cooled PBS.

Cell extracts are prepared by rinsing cells twice with ice-cold PBS/phosphatase inhibitor and gently puffing them to suspend them in 500 L of hypotonic buffer. After 15 min on ice, 25 L of detergent was added to the solution above to dissolve the proteins in the cytoplasm in the supernatant. After 30 seconds of centrifugation (4°C, 14,000×g), the nuclei pellet was collected. After collecting the fragments of nuclei, they were suspended in 50L of complete lysis buffer and incubated on ice for 30 min. After centrifugation, the supernatant was collected for further analysis.

2.3 Preparation of MIP sensor

Three steps were used to pre-treat the Au electrode: (1) The Au electrode was polished to a mirror surface with 0.05 μm Al_2O_3. (2) The electrode was ultrasonically cleaned in anhydrous ethanol and secondary distilled water for 5 min. (3) The electrode was scanned cyclically voltammetrically from -0.1 V to 1.5 V for ten cycles (scab speed 100 mV/s) in 0.5 M H_2SO_4 solution. After immersing the cleaned electrode in a 50 mM p-ATP ethanol solution for 24 hours at room temperature, the physically adsorbed p-ATP was washed with ethanol and secondary distilled water (denoted as p-ATP/Au).

The modified gold electrode was immersed in an ethanol solution containing 10 mM p-ATP, 50 mM TBAP, 0.5 μM ER and 0.2 g/L $HAuCl_4$. The polymerization process was performed by scanning 10 turns in the potential range -0.3 V to 1.2 V (sweep rate: 50 mV/s, denoted as p-ATP-ER/Au). After electropolymerization, the composite membrane modified electrode was immersed in ethanol:water (4:1) containing 0.2 M HCl solution for 3 min to remove the template molecules (denoted as p-AuNPs-MIP/Au). The electrode with the template molecules removed was washed sequentially with ethanol and secondary distilled water and blown dry under nitrogen for later use.

3. RESULTS AND DISCUSSION

The imprinted p-AuNPs-MIP/Au electrode preparation process is illustrated in Figure 1. The preparation procedure can be summarized as follows: p-ATP self-assembly on the Au electrode surface; ER hydrogen bonding on the p-ATP-ER/Au electrode surface; AuNPs co-polymerization on the p-ATP-ER/Au electrode surface; and ER removal from the imprinted membrane. Prior to co-polymerization, the Au was immersed in p-ATP solution for 24 hours. The p-ATP self-assembles onto the gold electrode due to the Au-S bond formed between the p-sulfhydryl ATP's group and the gold electrode [32,33]. Prior to electropolymerization, the p-ATP film was chemisorbed onto the Au electrode surface, exposing a row of amino groups to the solution. Following that, the electrode was immersed in ER solution for 4 hours. By hydrogen bonding between the amino group in p-ATP and the oxygen in the ER, the ER was attached to the surface of the p-ATP-modified Au electrode [34]. Between the oxygen atoms in p-ATP and -NH2 in ER, there is a strong hydrogen bond [35]. As a result, the strong hydrogen bonding promotes ER attachment to the p-ATP/Au. These ER molecules assembled on the surface of the p-ATP/Au were

embedded into the membrane, forming surface imprinting sites that increase the number of imprinting sites and thus the sensitivity.

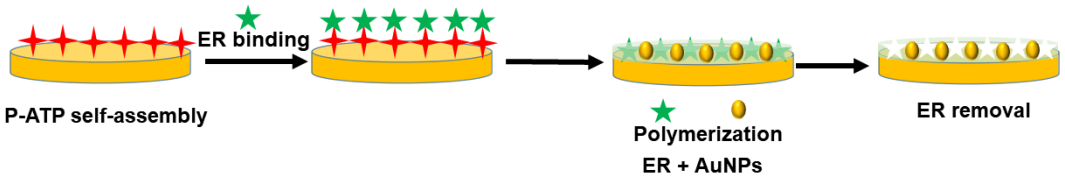

Figure 1. Schematic diagram of the preparation of p-AuNPs-MIP/Au.

The SEM images of modified p-AuNPs-MIP/Au are shown in Figure 2. As shown in the figure, AuNPs structures formed on the Au surface. The electrode surface of p-AuNPs-MIP/Au is fairly rough, and the nano-gold has a diameter of between 5 and 20 nm.

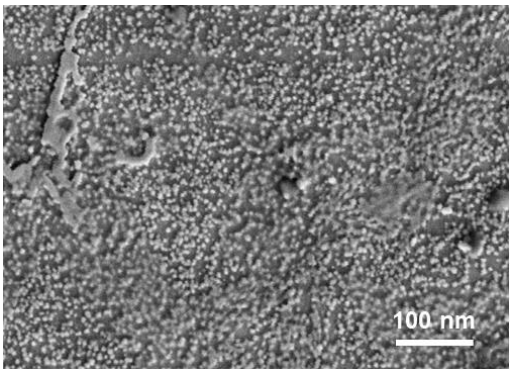

Figure 2. SEM image of p-AuNPs-MIP/Au.

To determine whether the modified electrode can recognize acetylsalicylic acid, it was immersed in 10 mM $[Fe(CN)_6]^{3-}$/$[Fe(CN)_6]^{4-}$ containing 0.1 mM KCl as the supporting electrolyte for cyclic voltammetry at various steps [36]. $[Fe(CN)_6]^{3-}$/$[Fe(CN)_6]^{4-}$ was used as a medium between the electrode and the substrate solution in this procedure. The relationship between the peak current and the modification of the Au electrode surface is depicted in Figure 3. A rapid decrease in the redox peak current is observed for the MIP-Au electrode, indicating the formation of a dense film on the Au electrode surface and its subsequent adsorption to the electrode surface [37]. After the template was removed, a distinct peak current was observed. The decrease in current from a to f demonstrates that the p-AuNPs composite was a conductive membrane, indicating that the modified electrode has a high sensitivity for acetylsalicylic acid detection. The appearance of curve c is ascribed to the MIP membrane obstructing electron transfer from $[Fe(CN)_6]^{3-}$/$[Fe(CN)_6]^{4-}$ following the newly bound ER [38]. Cyclic voltammetry was used to determine whether the modified electrode can recognize the ER. The MIP was

immersed in 10 mM $[Fe(CN)_6]^{3-}/[Fe(CN)_6]^{4-}$ containing 0.1 mM KCl. $[Fe(CN)_6]^{3-}/[Fe(CN)_6]^{4-}$ was used as a medium between the electrode and the substrate solution in this procedure.

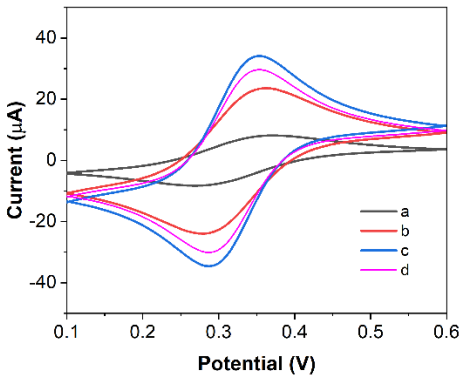

Figure 3. CVs of 10 mM $[Fe(CN)_6]^{3-}/[Fe(CN)_6]^{4-}$ and 0.1 M KCl at (a) p-ATP-ER/Au electrode, (b) p-AuNPs-MIP/Au, (c) p-AuNPs-MIP/Au after rebinding, (d) bare Au electrode.

It is well established that different pre-enrichment and elution times produce distinct EIS responses [39,40]. The following kinetic experiments were conducted to determine the optimal operating time for the detection of ER. Figure 4A illustrates the resistance variation as the accumulation time was varied. Due to the fact that the presence of ER inhibits the transfer of $[Fe(CN)_6]^{3-}/[Fe(CN)_6]^{4-}$ ion pairs to the electrode surface, different EIS curves were collected when p-AuNPs-MIP/Au was immersed in the same concentration of ER solution for varying periods of time [41]. The impedance increases as the accumulation time increases, and the adsorption equilibrium was reached after 200 s. As a result, accumulating for 200 s prior to ER detection maximizes response.

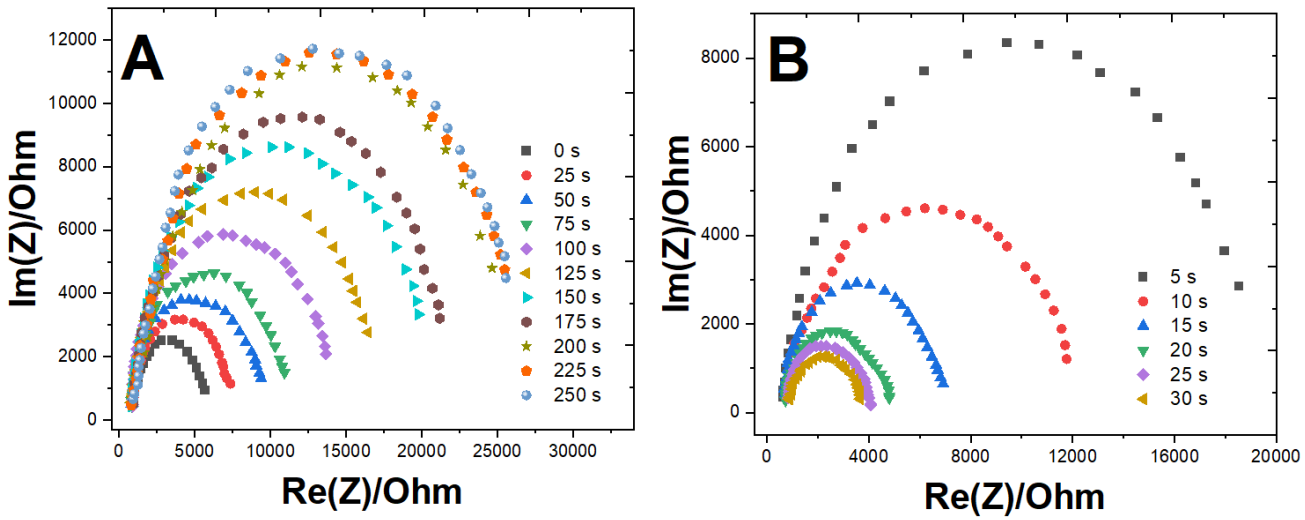

Figure 4. Effect of different (A) accumulation period and washing times towards p-AuNPs-MIP/Au in an ethanol acidic solution pH 5.2.

To determine the elution time, p-AuNPs-MIP/Au was immersed in an acidic solution of ethanol: water (4:1) and impedance spectroscopy was used to determine the elution time. As illustrated in Figure 4B, the impedance spectrum decreased gradually and stabilized at a minimum value after 80 s. As described previously, subsequent experiments used an accumulation time of 80 s and an elution time of 200 s.

For the quantitative analysis of ER detection, the p-AuNPs-MIP/Au was immersed for 200 s in various concentrations of ER solution. Figure 5 shows a significant increase in EIS. The results indicate that when the ER is newly bound, a dense film forms on the electrode surface, obstructing electron transfer of the $[Fe(CN)_6]^{3-}/[Fe(CN)_6]^{4-}$ ion pair. The values of $(c\text{-}c_0)/c_0$ and the ER concentration were plotted to obtain linear curves spanning the concentration range of 0.5 nM to 0.1 nM with a detection limit of 0.24 nM.

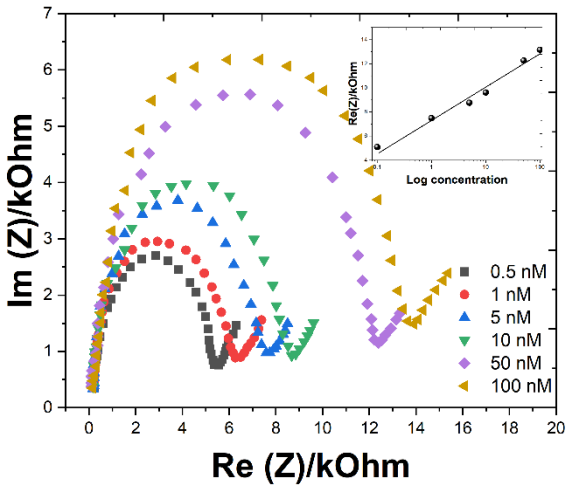

Figure 5. EIS of the p-AuNPs-MIP/Au to ER at different concentrations. Inset: A linear detection range was from 0.5 nM to 0.1 μM.

The effect of PI3K inhibitors on ER protein expression in breast cancer cells was investigated using the BT-474 cell line as a model. As illustrated in Figure 6A, the EIS curves generated by cells treated with BEZ-235 for 6 h were significantly smaller than those generated by cells treated with DMSO. These results indicate that PI3K inhibitors can increase the concentration of ER in the nucleus, indicating that they can reverse ER expression. To further investigate the relationship between ER protein expression and PI3K pathway inhibitors [42], we monitored changes in ER expression levels following treatment of BT474 cells with increasing concentrations of BEZ-235. We observed that as the concentration of BEZ-235 increased, the impedance value decreased. This is because the PI3K pathway directly suppresses ER expression in BT-474 cells [43], whereas increasing the concentration of BEZ-235 inhibits the PI3K pathway and thereby increases the concentration of ER in the nucleus. This dose-dependent expression of ER indicates a close relationship between the ER and PI3K pathways.

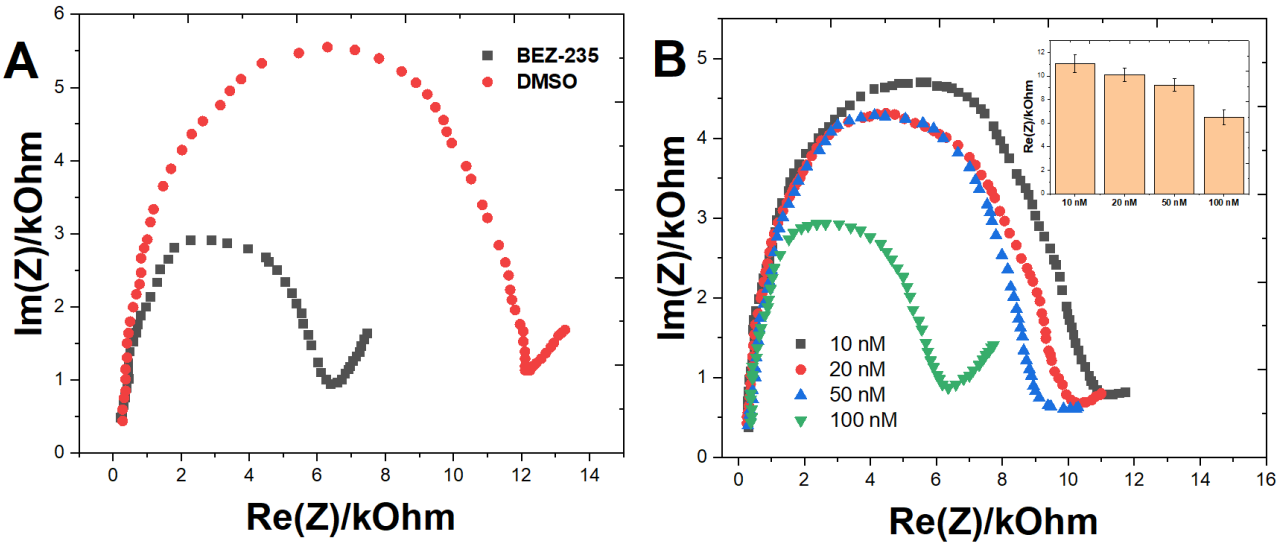

Figure 6. (A) EIS curves of p-AuNPs-MIP/Au toward DMSO treated cells and BEZ-235 treated cells. (B) The relationship between different concentrations of BEZ-235 and impedance values.

4. CONCLUSION

We developed an electrochemical biosensor for the detection of estrogen receptors. This sensor exhibits a high degree of sensitivity and specificity. Electropolymerization of the template molecule ER on the surface of P-AuNPs/Au occurs in the presence of the template molecule ER. To form binding sites, ER molecules are assembled into the P-AuNPs/Au imprinted membrane. The electrode surface assembly of nanoparticles results in a high specific surface area and excellent biocompatibility. We further investigated the relationship between ER expression levels and PI3K inhibitors in ER-positive breast cancers based on this effective electrochemical detection performance.

References

1. Y. Zhao, L. He, Y. Zhang, J. Zhao, Z. Liu, F. Xing, M. Liu, Z. Feng, W. Li and J. Zhang, *The Journal of Steroid Biochemistry and Molecular Biology*, 174 (2017) 96.
2. B. Zhang, J. Zhang, C. Zhang, X. Zhang, J. Ye, S. Kuang, G. Sun and X. Sun, *Frontiers in Pharmacology*, 9 (2018) 1227.
3. Z. Wang, Z. Pan, C. Xu and Z. Li, *Biochemical and Biophysical Research Communications*, 482 (2017) 948.
4. Z. Xu, M. Peng, Z. Zhang, H. Zeng, R. Shi, X. Ma, L. Wang and B. Liao, *Frontiers in Chemistry*, 9 (2021) 683.
5. W. Li, W. Luo, M. Li, L. Chen, L. Chen, H. Guan and M. Yu, *Frontiers in Chemistry*, 9 (2021) 610.
6. H. Karimi-Maleh, Y. Orooji, F. Karimi, M. Alizadeh, M. Baghayeri, J. Rouhi, S. Tajik, H. Beitollahi, S. Agarwal and V.K. Gupta, *Biosensors and Bioelectronics* (2021) 113252.
7. C.V. Uliana, C.R. Peverari, A.S. Afonso, M.R. Cominetti and R.C. Faria, *Biosensors and Bioelectronics*, 99 (2018) 156.
8. Z.S. Ulhaq and C.P. Garcia, *Acta Neurologica Belgica*, 121 (2021) 1281.
9. C.M. Tressler and N.J. Zondlo, *Biochemistry*, 56 (2017) 1062.

10. J. Zhou, Y. Zheng, J. Zhang, H. Karimi-Maleh, Y. Xu, Q. Zhou, L. Fu and W. Wu, *Analytical Letters*, 53 (2020) 2517.
11. H. Karimi-Maleh, A. Khataee, F. Karimi, M. Baghayeri, L. Fu, J. Rouhi, C. Karaman, O. Karaman and R. Boukherroub, *Chemosphere* (2021) 132928.
12. Y. Zheng, Y. Huang, H. Shi and L. Fu, *Inorganic and Nano-Metal Chemistry*, 49 (2019) 277.
13. X. Zhang, R. Yang, Z. Li, M. Zhang, Q. Wang, Y. Xu, L. Fu, J. Du, Y. Zheng and J. Zhu, *Revista Mexicana de Ingeniería Química*, 19 (2020) 281.
14. C. Li and F. Sun, *Frontiers in Chemistry*, 9 (2021) 409.
15. N. Sritana, T. Suriyo, J. Kanitwithayanun, B.H. Songvasin, A. Thiantanawat and J. Satayavivad, *Food and Chemical Toxicology*, 118 (2018) 595.
16. A. Nezami, R. Nosrati, B. Golichenari, R. Rezaee, G.I. Chatzidakis, A.M. Tsatsakis and G. Karimi, *TrAC Trends in Analytical Chemistry*, 94 (2017) 95.
17. Z. Zhang, M. Peng, D. Li, J. Yao, Y. Li, B. Wu, L. Wang and Z. Xu, *Frontiers in Chemistry*, 9 (2021) 702.
18. R. Mesnage, A. Phedonos, M. Biserni, M. Arno, S. Balu, J.C. Corton, R. Ugarte and M.N. Antoniou, *Food and Chemical Toxicology*, 108 (2017) 30.
19. R. Kase, B. Javurkova, E. Simon, K. Swart, S. Buchinger, S. Könemann, B.I. Escher, M. Carere, V. Dulio and S. Ait-Aissa, *TrAC Trends in Analytical Chemistry*, 102 (2018) 343.
20. H. Karimi-Maleh, F. Karimi, L. Fu, A.L. Sanati, M. Alizadeh, C. Karaman and Y. Orooji, *Journal of Hazardous Materials*, 423 (2022) 127058.
21. W. Wu, M. Wu, J. Zhou, Y. Xu, Z. Li, Y. Yao and L. Fu, *Sensors and Materials*, 32 (2020) 2941–2948.
22. W. Long, Y. Xie, H. Shi, J. Ying, J. Yang, Y. Huang and H. Zhang, L. Fu, *Fullerenes, Nanotubes and Carbon Nanostructures*, 26 (2018) 856–862.
23. Y. Wang, B. Pan, M. Zhang, X. Du, W. Wu, L. Fu, W. Zhou and Y. Zheng, *Analytical Sciences* (2020) 20P079.
24. R. Jeselsohn, C. De Angelis, M. Brown and R. Schiff, *Current Oncology Reports*, 19 (2017) 35.
25. L. Hsu, N. Chu and S. Kao, *International Journal of Molecular Sciences*, 18 (2017) 1713.
26. Z. Du, X. Feng, N. Li, J. Qu, L. Feng, L. Chen and W. Chen, *Phytomedicine*, 43 (2018) 11.
27. L. Yang, Q. Meng, Z. Hu, W. Ning, J. Zheng, C. Dong and H. Zhou, *Sensors and Actuators B: Chemical*, 272 (2018) 589.
28. M. Yagishita, T. Kubo, T. Nakano, F. Shiraishi, T. Tanigawa, T. Naito, T. Sano, S.F. Nakayama, D. Nakajima and K. Otsuka, *Chemosphere*, 217 (2019) 204.
29. L. Fu, K. Xie, Y. Zheng, L. Zhang and W. Su, *Electronics*, 7 (2018) 15.
30. R.M. Pallares, L. Sutarlie, N.T. Thanh and X. Su, *Sensors and Actuators B: Chemical*, 271 (2018) 97.
31. J. Li, K. Hu, Y. Zhang, Z. Zhang and Y. Yang, *Analytica Chimica Acta*, 1086 (2019) 110.
32. M. Ramezanzadeh, G. Bahlakeh, Z. Sanaei and B. Ramezanzadeh, *Applied Surface Science*, 463 (2019) 1058.
33. T.F. Otero and S. Beaumont, *Electrochimica Acta*, 257 (2017) 403.
34. S. Lv, K. Zhang, L. Zhu, D. Tang, R. Niessner and D. Knopp, *Analytical Chemistry*, 91 (2019) 12055–12062.
35. S. Kumaravel, T. Balamurugan, S. Jia, H. Lin and S. Huang, *Analytica Chimica Acta*, 1106 (2020) 168.
36. H.K. Kaya, S. Cinar, G. Altundal, Y. Bayramlı, C. Unaleroglu and F. Kuralay, *Sensors and Actuators B: Chemical*, 346 (2021) 130425.
37. F. El-Hajjaji, M. Messali, A. Aljuhani, M. Aouad, B. Hammouti, M. Belghiti, D. Chauhan and M. Quraishi, *Journal of Molecular Liquids*, 249 (2018) 997.
38. T. Balamurugan, C. Huang, P. Chang and S. Huang, *Analytical Chemistry*, 90 (2018) 12631.

39. A. Moradi, Z. Ranjbar, L. Guo, S. Javadpour and B. Ramezanzadeh, *Journal of Molecular Liquids*, 338 (2021) 116606.
40. Z. Huang, X. Li, Z. Wang, L. Hu, X. Tu and Y. Hu, *Journal of Molecular Liquids*, 343 (2021) 117615.
41. T.F. Otero, *Null*, 8 (2017) 125.
42. Maged.W. Helmy, A.I. Ghoneim, M.A. Katary and R.K. Elmahdy, *Molecular Biology Reports*, 47 (2020) 2217.
43. R. Nanta, A. Shrivastava, J. Sharma, S. Shankar and R.K. Srivastava, *Molecular and Cellular Biochemistry*, 454 (2019) 11.